Magnetic Resonance in Medicine 49:710–715 (2003)

Phased-Array MRI of Canine Prostate Using Endorectal and Endourethral Coils

Andrew C. Yung,[1] Ali Y. Oner,[1] Jean-Michel Serfaty,[1] Mark Feneley,[1] Xiaoming Yang,[1] and Ergin Atalar[1,2*]

A four-channel phased array consisting of one surface coil, two endorectal coils, and one flexible endourethral loop coil was designed for MRI of the canine prostate. The endorectal coils provide high signal in the posterior region of the prostate, while the endourethral and surface coils are sensitive to the central and anterior regions of the prostate. Gel phantom experiments indicate that the proposed phased-array configuration generates 15 times more signal-to-noise ratio (SNR) than a combination of two surface coils and one endorectal coil within the posterior region of the prostate; the performance of the two configurations is comparable near the anterior prostate surface. Ultimate intrinsic SNR (UISNR) analysis was used to compare the proposed phased array's performance to the best possible SNR for external coils. This analysis showed that the proposed phased array outperforms the best-case external coil within the posterior and central regions of the prostate by up to 20 times. In canine experiments in vivo, high-resolution fast spin-echo (FSE) images of the prostate were obtained with a pixel size of 230 μm obtained in 3 min 12 s. The proposed phased-array design potentially can be used to increase the accuracy of prostate cancer staging and the feasibility of MR-guided prostate interventions. Magn Reson Med 49:710–715, 2003. © 2003 Wiley-Liss, Inc.

Key words: prostate MRI; phased array; flexible endourethral loop coil; endorectal coil; ultimate intrinsic SNR

MRI techniques have received much attention for their application to the visualization and treatment of prostate cancer, which is the second largest cause of cancer-related deaths in American men (1). The excellent soft-tissue contrast provided by MRI allows improved visualization of the prostate anatomy, surrounding critical structures (such as the neurovascular bundles and periurethral zone), and the extent of tumor spread. This improved contrast resolution presents a distinct advantage over other prostate imaging modalities such as transrectal ultrasound (TRUS) or CT. For example, prostate cancer does not have a uniform appearance in grayscale ultrasound images; some authors report that up to 56% of prostate carcinomas are in areas that appeared normal under TRUS (2). Consequently, MRI has been used in the management of prostate cancer as a tool for preoperative evaluation (3), cancer staging (4), and image guidance of prostate interventions (5–7). The current state-of-the-art techniques for prostate MRI use an endorectal coil (8), surface coils, or a combination of both (9).

However, current prostate MRI techniques do not provide sufficient image resolution to clearly visualize all features of interest. For example, lesions that are <5 mm in size are difficult to detect when endorectal imaging is used, with a sensitivity of only 10% (10). Endorectal MRI staging gives excellent specificity of extracapsular extension (95%) but suffers from low sensitivity (38%), in part because current methods cannot identify capsular penetrations of <1 mm (11). MR-guided prostate interventions may also suffer from limited image quality, especially during real-time procedures (when imaging time is short) and when the magnetic field strength of the scanner is low (which is often the case for interventional MR suites).

We believe that a higher signal-to-noise ratio (SNR) would improve the ability of MRI to stage prostate cancer, as well as increase the feasibility of MR-guided interventions of the prostate. To achieve this improvement in SNR, we developed a new four-channel phased-array design consisting of two endorectal coils, one endourethral coil, and one surface coil. The use of endourethral coils for prostate imaging is rather novel, and may be an important improvement over current methods because they offer enhanced signal sensitivity in the central region of the prostate. We also attempted to extend the state-of-the-art techniques for prostate MRI by using two rectal coils instead of one, in order to increase signal in the posterior portion of the gland.

To test our ideas, custom endourethral coils and endorectal coils were designed and constructed. In vivo canine experiments and phantom experiments were performed to test the proposed phased-array system, and to compare its performance with other coil configurations that are currently being used for prostate MRI.

METHODS

We constructed a flexible endourethral loop coil and a dual-coil endorectal probe for prostate imaging. Figure 1 shows how the coils are placed in a dog: The dual-coil endorectal probe is placed in the rectum and positioned along the posterior base of the prostate, while the endourethral coil is inserted into the prostatic urethra that runs through the central portion of the gland. An external surface coil is placed on the anterior pelvic surface of the dog.

Flexible Endourethral Loop Coil Design

The flexible endourethral loop coil (shown in Fig. 2a) is implemented as a flexible copper circuit mounted on a

[1]Department of Radiology, NMR Research Division, Johns Hopkins University School of Medicine, Baltimore, Maryland.

[2]Department of Electrical and Electronics Engineering, Bilkent University, Ankara, Turkey.

Grant sponsor: NIH; Grant number: R01 HL 57483; Grant sponsor: United States Army; Grant number: PC 001229.

*Correspondence to: Ergin Atalar, Ph.D., Department of Radiology, NMR Research Division, Johns Hopkins University School of Medicine, 720 Rutland Ave., Traylor Bldg., Rm. 330, Baltimore, MD 21205.
E-mail: eatalar@mri.jhu.edu

Received 16 August 2002; revised 25 October 2002; accepted 1 December 2002.

DOI 10.1002/mrm.10432
Published online in Wiley InterScience (www.interscience.wiley.com).

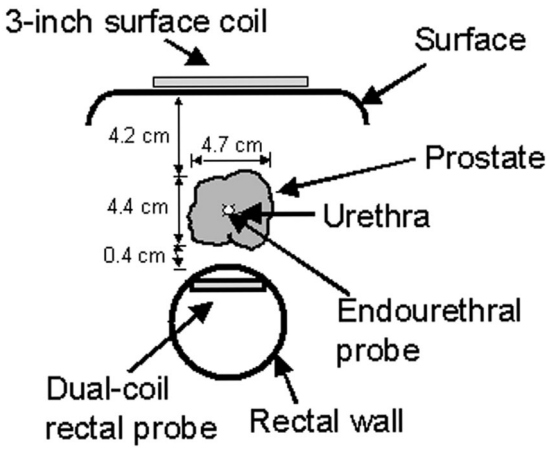

FIG. 1. Coil placement in a canine prostate, and approximate anatomical dimensions.

piece of polyimide film. The sensitive portion of the coil consists of an elongated loop measuring 5 cm in length, with a trace separation of 0.5 cm. Matching capacitors are mounted directly onto the flex circuit itself, in order to transform the coil impedance to the 50 ohms that the scanner preamplifiers expect. The series capacitance in the matching network is distributed over the loop. A decoupling PIN diode mounted on the flex circuit detunes the coil during RF transmission, thereby preventing the coil from interfering with the excitation flip angle. This is achieved by positioning the PIN diode at a certain distance away from the parallel capacitor, so that the line inductance will form a blocking resonance with the parallel capacitor when the PIN diode is switched on during transmit. To choke the ground currents, a quarter-wavelength "bazooka balun" constructed from copper tape was mounted on the coaxial cable that connects the antenna to the scanner. The entire assembly was placed inside a 16-Fr Foley catheter (5.3 mm outer diameter). A previous study of urethral imaging (12) used a similar design.

Dual-Coil Endorectal Probe Design

The endorectal imaging probe (Fig. 2b) consists of two etched loop coils mounted side by side on a printed circuit board. Each loop coil, along with its associated matching/detuning circuitry, is exactly analogous in design to the flexible endourethral loop coil described above. Each loop is rectangular in shape (24 mm × 14 mm), and the coils overlap each other in the lateral direction (jumper wires at the crossover points were used to bridge one coil trace over the other). The coils were mounted on a tapered silicone probe head (3 cm wide) attached to a 24-cm plastic handle, and then covered with a coat of protective plastic. In addition, bazooka baluns made out of copper tape were built on the coaxial cables connecting the coils to the scanner.

The need to reduce crosstalk between the two endorectal loop coils was an important consideration in the probe design. The coils were overlapped to reduce the amount of inductive crosstalk, and a strip of copper tape in the overlap region was used to block the remaining interloop net flux. The elimination of crosstalk was verified by measurements using a network analyzer.

Phantom Experiments

Phantom experiments were undertaken to measure the SNR performance of the coils, and to study electromagnetic interactions between elements of the phased array. The phantom was made from a cylindrical acrylic shell (20.4 cm inner diameter, 24 cm long) filled with polyacrylamide gel, with table salt added to approximate the electrical properties of living tissue (σ = 0.6 S/m, ϵ = 77.7). The coils were situated in such a way as to mimic their placement in a dog, as approximated by previous in vivo canine imaging experiments. Our proposed phased-array configuration (i.e., two endorectal coils, one flexible endourethral loop coil, and one surface coil) was used to acquire images of the gel phantom in a 1.5 T GE Signa scanner. Axial images were obtained using a spin-echo sequence that minimized T_1 and T_2 effects (TE/TR = 9/6000 ms, matrix = 256 × 128, NEX = 1, FOV = 22 cm, slice thickness = 1.5 mm). An alternative phased-array design was also investigated by replacing the flexible endourethral loop coil with an endourethral loopless antenna (2.5 mm in diameter). This design was originally used for transesophageal imaging of the aorta (13). For further comparisons, SNR tests were also performed on a phased array consisting of a Medrad Innervu 1.5T endo-

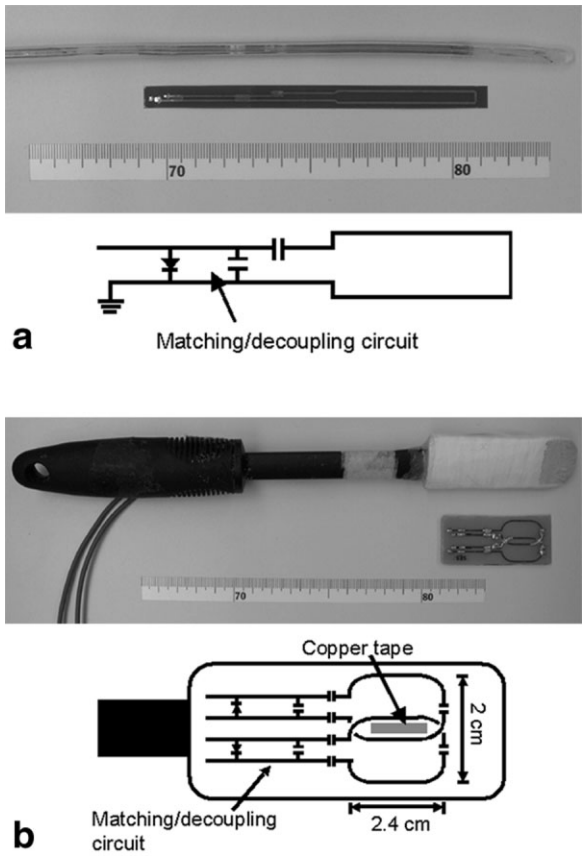

FIG. 2. Photographs and circuit schematics for (**a**) a flexible endourethral loop coil and (**b**) a dual-coil endorectal probe.

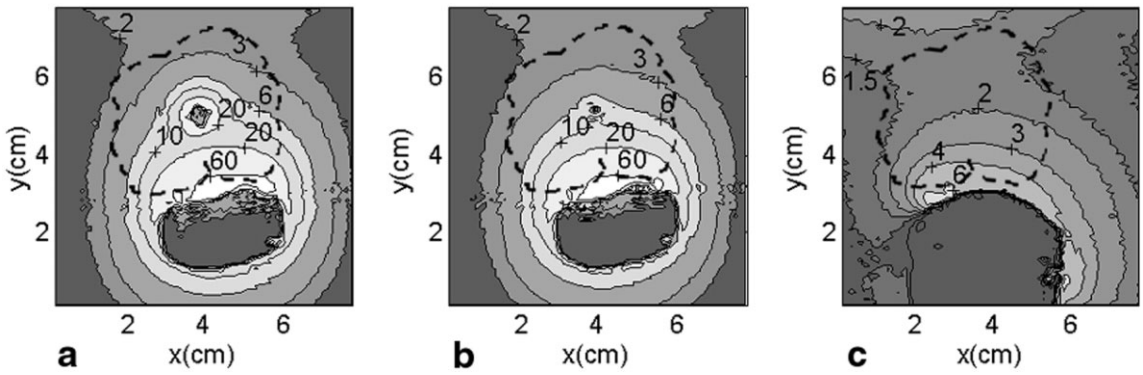

FIG. 3. SNR contour maps in a polyacrylamide phantom for (**a**) a flexible endourethral loop coil, dual-coil endorectal probe, 3-inch surface coil; (**b**) a loopless endourethral antenna, dual-coil endorectal probe, 3-inch surface coil; and (**c**) a Medrad endorectal coil, 3-inch surface coil (anterior), 5-inch surface coil (posterior). The dashed outline denotes the boundaries of the dog prostate.

rectal coil (with the balloon inflated), a 3-inch surface coil on the anterior surface, and a 5-inch surface coil on the posterior surface. This arrangement was used to mimic the endorectal-pelvic phased-array coil combination that is described in the literature (9). SNR maps of the resultant composite images were generated using the optimum reconstruction method, as described in Ref. 14. The amount of isolation between phased-array coil elements was also tested in the polyacrylamide phantom using a network analyzer.

As an additional measure of system performance, ultimate intrinsic SNR (UISNR) analysis (originally proposed by Ocali and Atalar (15)) was performed to determine the best possible SNR that can be produced by external surface coils. Assuming that only external coils are used, the UISNR method determines the best possible SNR for a particular sample geometry (in this case, the cylindrical phantom) by solving for the electromagnetic field that minimizes noise resistance in each voxel. The UISNR formulation originally proposed by Ocali and Atalar (15) used plane wave basis functions to determine the electromagnetic fields. For our purposes, we used cylindrical wave basis functions to construct the field equations. This was done to make the computation of the UISNR more numerically stable, given the phantom's cylindrical symmetry. The number of electromagnetic modes included in the computation was chosen so that any further addition of modes resulted in negligible change (1%) in the final result (13 angular modes and nine longitudinal modes). The UISNR for external surface coils was then compared to the experimentally obtained intrinsic SNR (ISNR) of the proposed phased array.

In Vivo Canine Studies

A series of canine studies ($N = 5$) was performed in a 1.5 T GE scanner. These experiments were conducted in accordance with all regulations set forth by the relevant institutional and governmental agencies. The dogs (weighing approximately 50 kg) were anesthetized throughout the procedure and positioned supine on the scanner bed, caudal end first. Large FOV scout images were acquired to help guide coil placement (as illustrated in Fig. 1) for maximum coverage of the prostate. The flexible endourethral loop coil was surgically inserted into the urethra through a percutaneous cut in the perineum, advanced into the prostatic urethra, and fixated in the prostate by inflating the balloon at the end of its Foley catheter. Once the coils were placed, the prostate was imaged with a series of T_1-weighted and T_2-weighted fast spin-echo (FSE) scans. The in vivo experiment images were reconstructed using the standard sum-of-squares reconstruction technique.

RESULTS

All of the coils matched well, as indicated by measured reflection coefficients ranging from 0.05 to 0.16 in magnitude.

Figure 3 shows phantom SNR measurements for our proposed phased-array system (with the loopless antenna replacing the endourethral loop coil in Fig. 3b), as well as for the combination of the Medrad endorectal coil and two surface coils. An outline of the prostate is shown on the figure to highlight the region of interest (ROI), and the contour values are percentages of the highest SNR value found in all three SNR maps. It is apparent that the loopless endourethral antenna (Fig. 3b) contributes only a small amount of additional SNR, whereas the flexible endourethral loop coil has a greater contribution to the overall signal profile within a diameter of approximately 2 cm around the urethra (Fig. 3a). A comparison of Fig. 3a and c shows that our new phased-array system produces an SNR gain of up to 15 times compared to the Medrad/surface coil combination, within the region of the canine prostate.

Figure 4 shows a coil performance map (CPM) that depicts the ratio between the ISNR produced by our proposed phased-array system and the UISNR for external coils. It is important to note that only internal coils can achieve CPM values of >1, while the CPM values of physically realizable external coils are always <1 (for example, the literature shows cases of external surface coils that produce CPM values of up to 0.8 at certain locations (15)). Within the posterior and central regions of the prostate, the proposed phased-array system performs up to 20 times better than the best-case external surface coil.

Isolation between the two rectal coils was measured to be 23 dB, indicating that good decoupling was achieved.

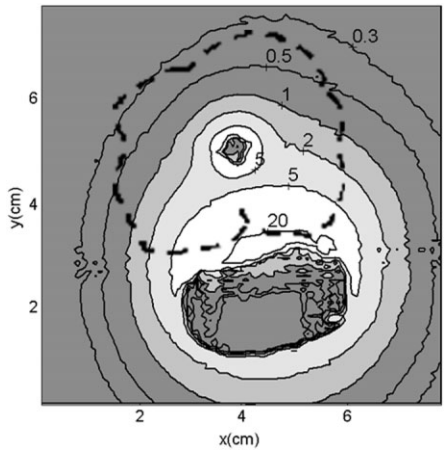

FIG. 4. CPM in a polyacrylamide phantom comparing the prostate phased array SNR with the UISNR for external coils.

Isolation between the flexible endourethral loop coil and other elements in the phased array was dependent on the endourethral coil orientation, and values ranged from 18 to 25 dB. Overall, isolation between coil elements (when tested in the polyacrylamide phantom) was at least 18 dB. In addition, the B_1 distortions in the individual channels were evaluated by two radiologists (J.M.S. and A.Y.O.) and deemed acceptable. The most significant distortion was found in the loop endourethral coil component image, where a "shadow" near the rectal coils was observed. However, the level of this artifact was at least 8–10 times smaller than the actual rectal coil signal.

Figure 5 shows a T_2-weighted axial image of a dog prostate that was generated by the flexible endourethral loop coil and the dual-coil rectal probe (pixel size = 230 μm, acquired in 3 min 12 s). The prostatic capsule and the walls of the urethra (i.e., the periurethral zone) can be seen clearly. A small circular feature that appears to be one of the neurovascular bundles can also be seen in the lower right corner of the image. The bright dot in the urethra

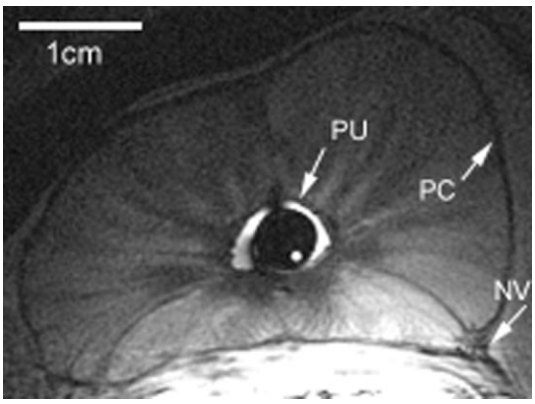

FIG. 5. Axial image of a dog prostate using the flexible endourethral loop coil and dual-coil endorectal probe. Sequence parameters: FSE; TR/TE = 3000/108 ms; FOV = 6 cm; slice thickness = 2 mm; NEX = 4; ETL = 16; matrix = 256 × 256. Arrows points to the periurethral zone (PU), the prostatic capsule (PC), and the possible location of the neurovascular bundle (NV).

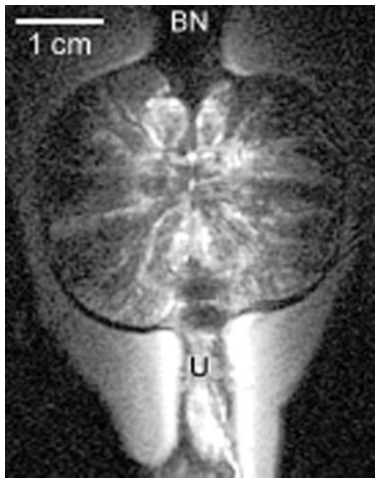

FIG. 6. Coronal image of a dog prostate using the flexible endourethral loop coil. Sequence parameters: FSE; TR/TE = 3500/102 ms; FOV = 8 cm; slice thickness = 2 mm; NEX = 8; ETL = 32; matrix = 256 × 256. The bladder neck (BN) and urethra (U) are visualized.

originated from water inside the Foley catheter's balloon inflation channel, which helped to indicate the orientation of the flexible endourethral loop coil. Figure 6 shows a coronal image of a different dog prostate that was acquired with the flexible endourethral loop coil alone. A pixel size of 310 μm was achieved in 3 min 44 s, with the bladder neck and urethra clearly depicted in the image.

DISCUSSION AND CONCLUSIONS

Increasing the sensitivity of the coil system is an effective way to achieve better MR images of the prostate. Better coil sensitivity may allow an increase in image resolution (without a concomitant increase in imaging time), which in turn allows the visualization of smaller anatomical features. This is especially important in detecting small tumors near the prostatic capsule, due to the increased probability of extraglandular diffusion in these tumors (16). A sensitive coil configuration is also important for increasing the SNR for MR-guided interventions of the prostate, since the field strength is often limited by the need for open magnets to allow for patient access. Again, precise localization of the tumor and the surrounding anatomy is necessary to ensure proper treatment of cancerous tissue while avoiding unwanted morbidity in surrounding critical structures. The desire to improve the performance of such interventional procedures was a direct motivation for our development of an optimized phased-array coil system for the prostate.

In our phased-array system design, the choice of coils was influenced by the geometry of the prostate and the surrounding anatomy. Specifically, each element in the array performs optimally in distinctly different regions of the prostate. The size and placement of the coils on the endorectal probe were chosen to optimize sensitivity in the posterior region of the prostate, while ensuring adequate coverage of the prostate along its entire lateral dimension. The endourethal coil provided high signal in the central part of the prostate along the entire length of the

prostatic urethra. In addition, the 3-inch surface coil was selected to contribute to the SNR in the anterior region of the prostate.

Phantom experiments indicate that the best SNR performance for a dog prostate geometry is produced when the phased array consists of two endorectal coils, one flexible endourethral loop coil, and one surface coil. The endorectal coils provide most of the signal, while the endourethral loop coil further adds to the signal over a diameter of approximately 2 cm around the urethra, as shown in Fig. 3a. Increasing the SNR around the urethra may be clinically important for imaging the central zone found in human prostates, where approximately 20% of the tumors occur (17). In cases in which imaging around the urethra is unimportant (e.g., during examinations of extracapsular extension), the endourethral coil may be omitted from the array. We used the Medrad endorectal/surface coil combination to represent the current state-of-the-art technique for prostate MRI (8). Our proposed phased-array system performed better by a factor of up to 15 times within the ROI. UISNR analysis predicted that the proposed phased-array system outperforms the best-case external surface coil in the posterior and central regions of the prostate, with an up to 20-fold improvement. However, the proposed phased-array system generates lower SNR in the anterior region of the prostate, which indicates that the SNR performance can still be improved. This improvement can be achieved by using multiple coils at the surface.

It is important to note that the choice of coils may change for a different prostate geometry or subject size. For example, the rectal coils are the most significant contributors of signal in the current system. However, if the patient or the prostate is of a larger size (which is often the case for human patients with benign prostatic hyperplasia), the endourethral coil may become more important in providing signal coverage within the prostate. A larger prostate may also make the loopless endourethral antenna a more attractive option, because the signal from a loopless antenna drops off more slowly with distance compared to the signal from the flexible loop version. A larger endorectal coil may also be necessary for a larger prostate.

The in vivo experimental images reveal a high level of anatomic detail, as shown in Figs. 5 and 6. The prostatic capsule, periurethral zone, and bladder neck were visualized in the experimental images, which may be clinically important in determining the extracapsular spread of the disease and preventing harm to such critical structures during interventions. A structure that appears to be the neurovascular bundle can also be identified in Fig. 5. It is especially important to visualize this structure during interventions, because impotence may result if the neurovascular bundle is damaged. Figure 6 shows that high-quality in vivo images can be obtained when only the endourethral loop coil is used. This offers an alternative to the current phased-array system if placement of coils inside the rectum is not possible, as a result of patient refusal, previous surgical resection of the rectum, or other complications in the rectum. Overall, high-quality in vivo images of the canine prostate were obtained with a pixel size as small as 230 μm, and an acquisition time of 3 min 12 s.

The results gleaned from the canine prostate model, while instructive, do not entirely mimic the situation in the human prostate. The canine prostate has none of the zonal anatomy that the human prostate possesses, and the distinction of these zones is important because cancer nodes are more likely to form in certain zones than in others (the peripheral zone in particular). There were also no cancer nodes in the canine prostates that we examined, and therefore the phased array's ability to identify cancerous tissue could not be tested in these experiments. Nevertheless, the current phased-array design may be valuable for animal studies that are performed in support of the development of new prostate imaging techniques and MR-guided prostate interventions (18).

Clearly, human studies must be performed to examine the phased array's utility in staging prostate cancer and guiding prostate interventions. As stated above, the coil geometries may need to be modified in order to account for the larger human prostate geometry. In terms of patient tolerance, the loopless endourethral antenna is attractive because of its small diameter. The flexible endourethral loop coil size also seems acceptable, since 16-Fr Foley catheters are often used in clinical practice. The larger size of the human urethra obviates the need for surgical insertion of the flexible endourethral loop coil into the prostate. The mechanical compliance of the rectal probe may need to be improved before this probe is used in humans.

We believe that the array coils for a human would be comparable in size to the coils used in the current design. In our canine subjects, the separation between the anterior pelvic surface and the prostate was comparable to dimensions found in average human males. For example, this separation distance in the male dataset of the Visible Human Project (19) measured as little as 5.4 cm (as compared to 4.2 cm in the canines). The examined canine prostates were also similar in size to normal adult human prostates (roughly 3 cm $\times$ 4.5 cm $\times$ 4 cm (17)). In more clinically relevant cases, prostates are larger as a result of benign prostatic hyperplasia. However, the design philosophy of a phased-array system for clinical human use would be the same as the design presented in this work, i.e., the use of multiple small endorectal coils to image the posterior region of the prostate, and surface coils and a loop endourethral coil to add signal in the central and anterior regions of the prostate.

ACKNOWLEDGMENTS

The authors thank Mary McAllister for assistance with manuscript preparation. The authors are also grateful to Ken Rent for preparation of the animals, and to Robert C. Susil for technical advice.

REFERENCES

1. Jemal A, Thomas A, Murray T, Thun M. Cancer statistics, 2002. CA Cancer J Clin 2002;52:23–47.
2. Ellis WJ, Brawer MK. The significance of isoechoic prostatic carcinoma. J Urol 1994;152(6 Pt 2):2304–2307.
3. Sanchez-Chapado M, Angulo JC, Ibarburen C, Aguado F, Ruiz A, Viano J, Garcia-Segura JM, Gonzalez-Esteban J, Rodriquez-Vallejo JM. Comparison of digital rectal examination, transrectal ultrasonography, and multicoil magnetic resonance imaging for preoperative evaluation of prostate cancer. Eur Urol 1997;32:140–149.

4. Smith Jr JA, Scardino PT, Resnick MI, Hernandez AD, Rose SC, Egger MJ. Transrectal ultrasound versus digital rectal examination for the staging of carcinoma of the prostate: results of a prospective, multi-institutional trial. J Urol 1997;157:902–906.
5. Porter AT, Blasko JC, Grimm PD, Reddy SM, Ragde H. Brachytherapy for prostate cancer. CA Cancer J Clin 1995;45:165–178.
6. Yerushalmi A. Localized, non-invasive deep microwave hyperthermia for the treatment of prostatic tumors: the first 5 years. Recent Results Cancer Res 1988;107:141–146.
7. Pisters LL, von Eschenbach AC, Scott SM, Swanson DA, Dinney CP, Pettaway CA, Babaian RJ. The efficacy and complications of salvage cryotherapy of the prostate. J Urol 1997;157:921–925.
8. Schnall MD, Imai Y, Tomaszewski J, Pollack HM, Lenkinski RE, Kressel HY. Prostate cancer: local staging with endorectal surface coil MR imaging. Radiology 1991;178:797–802.
9. Hricak H, White S, Vigneron D, Kurhanewicz J, Kosco A, Levin D, Weiss J, Narayan P, Carroll PR. Carcinoma of the prostate gland: MR imaging with pelvic phased-array coils versus integrated endorectal—pelvic phased-array coils. Radiology 1994;193:703–709.
10. Ikonen S, Karkkainen P, Kivisaari L, Salo JO, Taari K, Vehmas T, Tervahartiala P, Rannikko S. Magnetic resonance imaging of clinically localized prostatic cancer. J Urol 1998;159:915–919.
11. Jager GJ, Ruijter ET, van de Kaa CA, de la Rosette JJ, Oosterhof GO, Thornbury JR, Barentsz JO. Local staging of prostate cancer with endorectal MR imaging: correlation with histopathology. Am J Roentgenol 1996;166:845–852.
12. Quick HH, Serfaty JM, Pannu HK, Genadry R, Yeung CJ, Atalar E. Endourethral MRI. Magn Reson Med 2001;45:138–146.
13. Shunk KA, Lima JA, Heldman AW, Atalar E. Transesophageal magnetic resonance imaging. Magn Reson Med 1999;41:722–726.
14. Roemer PB, Edelstein WA, Hayes CE, Souza SP, Mueller OM. The NMR phased array. Magn Reson Med 1990;16:192–225.
15. Ocali O, Atalar E. Ultimate intrinsic signal-to-noise ratio in MRI. Magn Reson Med 1998;39:462–473.
16. Bartolozzi C, Crocetti L, Menchi I, Ortori S, Lencioni R. Endorectal magnetic resonance imaging in local staging of prostate carcinoma. Abdom Imaging 2001;26:111–122.
17. Wong-You-Cheong JJ, Krebs TL. MR imaging of prostate cancer. Magn Reson Imaging Clin N Am 2000;8:869–886.
18. Susil RC, Derbyshire JA, Krieger A, Tanacs A, Solaiyappan M, Whitcomb LL, McVeigh E, Fichtinger G, Atalar E. A realtime MRI system for guidance and monitoring of prostate biopsy. In: Proceedings of the 10th Annual Meeting of ISMRM, Honolulu, 2002. p 2237.
19. Ackerman MJ, Yoo T, Jenkins D. From data to knowledge—the Visible Human Project continues. Medinfo 2001;10(Pt 2):887–890.